Structural bifurcation for ductile necking localization

Shigenobu Okazawa *

Department of Social and Environmental Engineering, Hiroshima University, Higashi-Hiroshima, Hiroshima 739-8527, Japan

Abstract

Necking localization is common unstable behavior in ductile solids. This paper describes the unified necking localization mechanism. After describing one-dimensional instability problem, general material and structural instability criteria are formulated and the formulation is validated by non-linear finite element analysis. The trigger of necking localization is structural bifurcation and the behavior from a uniformly deformed state to ultimate localization just before fracture is continuous structural instability.

Key words: Stability; Bifurcation; Necking localization; Plasticity; Non-linear finite element method; Ductile solid

1 Introduction

A ductile solid shows unstable behavior from a uniformly deformed state to ultimate fracture through necking and localization after a peak point. This behavior is accepted as a fundamental cause not only of material but also of structural instability. Therefore, explaining necking localization in detail is a prerequisite for understanding the ultimate characteristics of ductile solids, and for investigating structural performances.

There are two approaches for computational simulation to allow for necking localization. The first is using constitutive modeling; for which various phenomenological constitutive models. For example, the deformation theory [1], the micro void model [2] or the thermal-softening capability model [3]. A

* Corresponding author. Tel: +81-82-424-7810; Fax: +81-82-422-7194
Email address: okazawa@hiroshima-u.ac.jp (Shigenobu Okazawa *).

great deal of related computational techniques have also been developed to simulate the shear band formation leading to the ultimate fracture [4][5][6][7]. The other approach is through structural instability. Structural instability is discussed as a bifurcation problem with a tangent stiffness matrix of a finite element method. The structural instability originates in geometrical nonlinear property; for example, structural buckling is its instability. Hill and Hutchinson [8] developed plastic bifurcation theory in ductile experiments based on Hill's uniqueness stability theory [9]. Thus Hill and Hutchinson's theory [8] has been applied to bifurcation analyses without imperfection [10][11]. Although conventional necking localization analyses have tended to depend on material instability, here I deal with necking localization analyses only within a framework of structural instability.

This paper presents a unified necking localization mechanism of ductile solids using structural bifurcation approach. After describing one-dimensional plastic instability theory, material and structural instability criteria are formulated. The present necking localization mechanism is validated by a proposed computational strategy without imperfection.

2 Plastic instability theory

2.1 Concept of Plastic Instability

Fig.1 shows an equilibrium one-dimensional ductile member. Letting the true stress, the cross-sectional area and the applied force be σ, a and P respectively, the equilibrium equation is as follows.

$$\sigma a = P \tag{1}$$

As the applied force P increases, the ductile member elongates and the cross-sectional area decreases. In general ductile solid, a plastic hardening tangent decreases gradually in a strain hardening zone. When an increment of the true stress σ cannot overtake an increment of the cross-sectional area a, the left side of Eq. (1) starts decreasing even with the hardening true stress relationship [12].

A peak point can occur even with the hardening true stress relationship with a uniformly deformed state. This phenomenon is not material softening because this instability originates from cross-sectional transformation. This is the reason why large deformation analysis is indispensable to simulate a decrease in the applied force of plastic instability behavior.

2.2 Peak Point of Power-Law Hardening Solid

Fig.2 shows a large deformation of a ductile member assuming constant volume with a square cross-section. Letting the Cauchy stress tensor, the first Piola-Kirchhoff stress tensor and the deformation gradient tensor be $\boldsymbol{\sigma}$, $\boldsymbol{\Pi}$ and $\boldsymbol{F}$ respectively, their relationship is,

$$\boldsymbol{\sigma} = \frac{1}{J}\boldsymbol{F} \cdot \boldsymbol{\Pi} \tag{2}$$

where J is the rate of volume change and is written with $\boldsymbol{F}$.

$$J = det\boldsymbol{F} \tag{3}$$

We assume a constant volume, J is equal to 1. The Cauchy stress tensor $\boldsymbol{\sigma}$ and the first Piola-Kirchhoff stress tensor $\boldsymbol{\Pi}$ are called the true stress tensor and the nominal stress tensor, respectively.

The components of $\boldsymbol{\sigma}$, $\boldsymbol{\Pi}$ and $\boldsymbol{F}$ in the three-dimensional Euclidean space of Fig. 2 are as follows, with basis vectors $\boldsymbol{e}_i$.

$$\boldsymbol{\sigma} = \frac{P}{h^2}\boldsymbol{e}_1 \otimes \boldsymbol{e}_1 \tag{4}$$

$$\boldsymbol{\Pi} = \frac{P}{H^2}\boldsymbol{e}_1 \otimes \boldsymbol{e}_1 \tag{5}$$

$$\boldsymbol{F} = \frac{l}{L}\boldsymbol{e}_1 \otimes \boldsymbol{e}_1 + \frac{h}{H}\boldsymbol{e}_2 \otimes \boldsymbol{e}_2 + \frac{h}{H}\boldsymbol{e}_3 \otimes \boldsymbol{e}_3 \tag{6}$$

Where P is the applied force. The nominal strain ε_n and the true strain ε_t are,

$$\varepsilon_n = \frac{l - L}{L} \tag{7}$$

$$\varepsilon_t = ln(1 + \varepsilon_n) \tag{8}$$

The following relationship is derived from Eqs. (7) and (8).

$$h^2 = H^2 e^{-\varepsilon_t} \tag{9}$$

The equilibrium equation for a component of the Cauchy stress σ_{11} is,

$$\sigma_{11} = \frac{P}{h^2} = \frac{P}{H^2}e^{\varepsilon_t} \tag{10}$$

Now I introduce a n-th power-law hardening as follows.

$$\sigma_{11} = k{\varepsilon_t}^n \tag{11}$$

where k is constant.

The hardening rate is calculated from Eq. (11).

$$\frac{\partial \sigma_{11}}{\partial \varepsilon_t} = \frac{\sigma_{11} n}{\varepsilon_t} \tag{12}$$

The incremental rate of σ_{11} calculated from Eq. (10).

$$\frac{\partial \sigma_{11}}{\partial \varepsilon_t} = \frac{P}{H^2} e^{\varepsilon_t} = \sigma_{11} \tag{13}$$

When the hardening rate cannot overtake the incremental rate of σ_{11}, the applied force starts to decrease. Then the peak point criterion in this case is,

$$n = \varepsilon_t \tag{14}$$

The peak point occurs even with a uniformly deformed state.

3 Material instability

The previous section shows that the applied force can decrease the uniform ductile member even with the hardening true stress-strain relationship. This section extends the availability of this instability criterion to general solid.

3.1 Material instability theory for infinitesimal deformation

In classical material instability theory, the stability criterion is the positive of a inner-product with material time derivatives of the infinitesimal strain $\boldsymbol{\varepsilon}$ and the Cauchy stress $\boldsymbol{\sigma}$ [13].

$$\dot{\boldsymbol{\epsilon}} : \dot{\boldsymbol{\sigma}} > 0 \tag{15}$$

The superscript $\cdot$ shows the material time derivative. "rate" is used instead of "material time derivative" for simplicity in the page that follow. I assume a constitutive relationship between the Cauchy stress rate $\dot{\boldsymbol{\sigma}}$ and the infinitesimal strain rate $\dot{\boldsymbol{\epsilon}}$ by using the 4th order constitutive tensor $\boldsymbol{C}$.

$$\dot{\boldsymbol{\sigma}} = \boldsymbol{C} : \dot{\boldsymbol{\epsilon}} \tag{16}$$

The stability criterion is derived by substituting the constitutive equation (16) for the inequality (15).

$$\dot{\boldsymbol{\epsilon}} : (\boldsymbol{C} : \dot{\boldsymbol{\epsilon}}) > 0 \tag{17}$$

Mathematically, the stability criterion (17) means the positive definite value of $\boldsymbol{C}$. Contrarily, the negative definite value of $\boldsymbol{C}$ shows material instability. This implies that the material instability criterion is as follows.

$$\det \boldsymbol{C} = 0 \tag{18}$$

3.2 Material instability theory for a large deformation

The stability criterion (15) is extended to be applicable to the problem of a large deformation. The instability criterion (15) uses infinitesimal strain and Cauchy stress. The other conjugate relationship, which is equivalent to (15), is indispensable for the stability criterion in the large deformation problem.

Let $\boldsymbol{X}$ and $\boldsymbol{x}$ be material coordinates before and after deformation $\boldsymbol{u}$.

$$\boldsymbol{x} = \boldsymbol{X} + \boldsymbol{u} \tag{19}$$

From the point of view of the large deformation problem, the infinitesimal strain tensor $\boldsymbol{\varepsilon}$ is the linear part of the Almansi strain tensor.

$$\boldsymbol{\epsilon} = \boldsymbol{A}_{(L)} = \frac{1}{2}\{\boldsymbol{u} \otimes \boldsymbol{\nabla}_x + (\boldsymbol{u} \otimes \boldsymbol{\nabla}_x)^T\} \tag{20}$$

Where $\boldsymbol{A}_{(L)}$ is the linear part of the Almansi strain tensor $\boldsymbol{A}$. By using the first Piola-Kirchhoff stress tensor $\boldsymbol{\Pi}$, the stability criterion, which is equivalent to the original stability criterion (15), is as follows.

$$(\dot{\boldsymbol{u}} \otimes \boldsymbol{\nabla}_x) : \dot{\boldsymbol{\sigma}} = \frac{1}{J}(\dot{\boldsymbol{u}} \otimes \boldsymbol{\nabla}_X) : \dot{\boldsymbol{\Pi}}^T > 0 \tag{21}$$

Where $\dot{\boldsymbol{u}}$ is the velocity vector. In addition, the stability criterion (21) can be rewritten to employ the second Piola-Kirchhoff stress tensors $\boldsymbol{S}$. The second Piola-Kirchhoff stress tensor is independent of rigid rotation.

$$\begin{aligned} &\frac{1}{J}(\dot{\boldsymbol{u}} \otimes \boldsymbol{\nabla}_X) : \dot{\boldsymbol{\Pi}}^T \\ &= \frac{1}{J}(\dot{\boldsymbol{u}} \otimes \boldsymbol{\nabla}_X) : (\dot{\boldsymbol{S}} \cdot \boldsymbol{F}^T + \boldsymbol{S} \cdot \dot{\boldsymbol{F}}^T)^T \\ &= \frac{1}{J}\left[\dot{\boldsymbol{S}} : \dot{\boldsymbol{E}} + \boldsymbol{S} : (\dot{\boldsymbol{F}}^T \cdot \dot{\boldsymbol{F}})\right] > 0 \end{aligned} \tag{22}$$

Where, the following relationship is used.

$$\boldsymbol{\Pi} = \boldsymbol{S} \cdot \boldsymbol{F}^T \tag{23}$$

And $\boldsymbol{E}$ is the Green Lagrange strain tensor and $\dot{\boldsymbol{E}}$ is as follows.

$$\dot{\boldsymbol{E}} = \frac{1}{2}\{(\dot{\boldsymbol{u}} \otimes \boldsymbol{\nabla}_X) + (\dot{\boldsymbol{u}} \otimes \boldsymbol{\nabla}_X)^T + (\dot{\boldsymbol{u}} \otimes \boldsymbol{\nabla}_X)^T \cdot (\dot{\boldsymbol{u}} \otimes \boldsymbol{\nabla}_X)\} \tag{24}$$

The updated Lagrangian formulation is generally effective in path-dependent large deformation analysis. In the updated Lagrangian formulation, the reference configuration is identical to the current configuration. Therefore, the following relationships are acceptable.

$$J = 1 \tag{25}$$

$$\boldsymbol{F} = \boldsymbol{I} \tag{26}$$

$$\dot{\boldsymbol{E}} = \boldsymbol{F}^T \cdot \boldsymbol{D} \cdot \boldsymbol{F} = \boldsymbol{D} \tag{27}$$

$$\dot{\boldsymbol{F}} = \boldsymbol{L} \cdot \boldsymbol{F} = \boldsymbol{L} \tag{28}$$

$$\boldsymbol{S} = \boldsymbol{\sigma} \tag{29}$$

Where $\boldsymbol{I}$ is the 2nd order unit tensor and $\boldsymbol{L}$ is the velocity gradient tensor.

$$\boldsymbol{L} = \dot{\boldsymbol{u}} \otimes \boldsymbol{\nabla}_x \tag{30}$$

Also $\boldsymbol{D}$ is the stretching tensor and the stretching tensor is a symmetric part of $\boldsymbol{L}$.

$$\boldsymbol{D} = \frac{1}{2}(\boldsymbol{L} + \boldsymbol{L}^T) \tag{31}$$

I derive the following inequality from Eq. (22) by considering Eqs. (25)-(29).

$$\dot{\boldsymbol{S}} : \boldsymbol{D} + \boldsymbol{\sigma} : (\boldsymbol{L}^T \cdot \boldsymbol{L}) > 0 \tag{32}$$

$\dot{\boldsymbol{S}}$ is generally called the Truesdell stress rate.

Next, I address the constitutive equation for the large strain problem. The constitutive equation for the large strain problem should have objectivity. In the constitutive equation (16) for the infinitesimal strain problem, the infinitesimal strain rate $\dot{\boldsymbol{\varepsilon}}$ can be replaced with the objective stretching tensor $\boldsymbol{D}$ and the Cauchy stress tensor rate $\dot{\boldsymbol{\sigma}}$ can be replaced with the objective stress rate. I select the Jaumann rate $\dot{\boldsymbol{\sigma}}^J$ because of the simple computational treatment among many objective stress rates. The constitutive equation with the Jaumann rate for the large strain problem is as follows.

$$\dot{\boldsymbol{\sigma}}^J = \boldsymbol{C} : \boldsymbol{D} \tag{33}$$

The stretching tensor $\boldsymbol{D}$ and the Jaumann rate of the Cauchy stress $\dot{\boldsymbol{\sigma}}^J$ are defined by an observer who moves along with the material deformation. This implies that the infinitesimal elasto-plastic theory is available even in the large strain problem by using the objective stress and strain rates.

The relationship between the Truesdell stress rate $\dot{\boldsymbol{S}}$ and the Jaumann rate of the Cauchy stress $\dot{\boldsymbol{\sigma}}^J$ is as follows.

$$\dot{\boldsymbol{S}} = \dot{\boldsymbol{\sigma}}^J - \boldsymbol{D}\cdot\boldsymbol{\sigma} - \boldsymbol{\sigma}\cdot\boldsymbol{D} + (\mathrm{tr}\boldsymbol{D})\,\boldsymbol{\sigma} \tag{34}$$

Although the 4th order constitutive tensor $\boldsymbol{C}$ is symmetric, the constitutive tensor between the Truedell stress rate $\dot{\boldsymbol{S}}$ and the stretching tensor $\boldsymbol{D}$ is asymmetric. The asymmetric constitutive tensor is unsuitable for application to a discussion of the stability criterion. Therefore, I redefine the constitutive equation using the Jaumann rate of relative Kirchhoff stress $\hat{\boldsymbol{\sigma}}$ instead of Cauchy stress.

$$\dot{\hat{\boldsymbol{\sigma}}}^J = \boldsymbol{C} : \boldsymbol{D} \tag{35}$$

The relationship between the Jaumann rate of Cauchy stress $\dot{\boldsymbol{\sigma}}^J$ and the Jaumann rate of relative Kirchhoff stress $\dot{\hat{\boldsymbol{\sigma}}}^J$ is as follows.

$$\dot{\hat{\boldsymbol{\sigma}}}^J = \dot{\boldsymbol{\sigma}}^J + (\mathrm{tr}\boldsymbol{D})\,\boldsymbol{\sigma} \tag{36}$$

The difference between $\dot{\boldsymbol{\sigma}}^J$ and $\dot{\hat{\boldsymbol{\sigma}}}^J$ is $(tr\boldsymbol{D})\,\boldsymbol{\sigma}$ and this difference can be neglected. This is because I assume incompressible plastic deformation and infinitesimal elastic deformation.

By using Eqs. (34) and (36), the relationship between the Truesdell stress rate $\dot{\boldsymbol{S}}$ and the Jaumann rate of relative Kirchhoff stress $\dot{\hat{\boldsymbol{\sigma}}}^J$ is as follows.

$$\dot{\boldsymbol{S}} = \dot{\hat{\boldsymbol{\sigma}}}^J - \boldsymbol{D}\cdot\boldsymbol{\sigma} - \boldsymbol{\sigma}\cdot\boldsymbol{D} \tag{37}$$

I derive the following constitutive equation by substituting Eq. (35) for (37).

$$\dot{\boldsymbol{S}} = \tilde{\boldsymbol{C}} : \boldsymbol{D} \tag{38}$$

Where $\tilde{\boldsymbol{C}}$ is the new 4th order constitutive tensor between the Truesdell stress rate $\dot{\boldsymbol{S}}$ and the stretching tensor $\boldsymbol{D}$. The index expression of $\tilde{\boldsymbol{C}}$ is as follows.

$$\tilde{C}_{ijkl} = C_{ijkl} - \frac{1}{2}(\delta_{il}\sigma_{kj} + \delta_{ik}\sigma_{lj}) - \frac{1}{2}(\sigma_{ik}\delta_{jl} + \sigma_{il}\delta_{jk}) \tag{39}$$

Where δ_{ij} is the Kronecker delta. $\tilde{C}_{ijkl}$ is the 4th symmetric tensor because $i\leftrightarrow j$, $k\leftrightarrow l$ and $i,j\leftrightarrow k,l$ are changeable in $\tilde{C}_{ijkl}$.

Substituting Eq. (38) for the stability criterion (32) yields,

$$\begin{aligned}\text{The left side of the inequality(32)} &= \boldsymbol{D} : (\tilde{\boldsymbol{C}} : \boldsymbol{D}) + \boldsymbol{\sigma} : (\boldsymbol{L}^T : \boldsymbol{L}) \\ &= \{\dot{u}\}^T[k]\{\dot{u}\} > 0\end{aligned} \tag{40}$$

In the inequality (40) ,

$$[k] = [k^m] + [k^g] \tag{41}$$

$$[k^m] = [b^m]^T[\tilde{C}][b^m] \tag{42}$$

$$[k^g] = [b^g]^T[\sigma][b^g] \tag{43}$$

$\boldsymbol{b}^m$ and $\boldsymbol{b}^g$ are the 3rd order tensors as follows.

$$\boldsymbol{D} = \boldsymbol{b}^m \cdot \dot{\boldsymbol{u}} \tag{44}$$

$$\boldsymbol{L} = \boldsymbol{b}^g \cdot \dot{\boldsymbol{u}} \tag{45}$$

$[b^m]$ and $[b^g]$ are suitable matrix indications of $\boldsymbol{b}^m$ and $\boldsymbol{b}^g$. Also $[\tilde{C}]$ and $[\sigma]$ are suitable matrix indications of $\tilde{\boldsymbol{C}}$ and $\boldsymbol{\sigma}$.

$[k]$ in the inequality (40) corresponds to the tangent stiffness on the material level of the updated Lagrangian formulation. The stability criterion (40) means the positive definite value of $[k]$. Therefore, the instability criterion is,

$$\det[k] = 0 \tag{46}$$

I can evaluate the peak point by using a determinant of the tangent stiffness of the material level before assembly. Additionally, a determinant of the assembled structural tangent stiffness matrix $[K]$ become zero simultaneously because the deformation state is uniform until the the peak point.

4 Structural instability

In the previous sections, I discussed the occurrence of the peak point using the material instability. In contrast to this, the material instability theory never describes the occurrence of necking immediately after the peak point. The structural instability theory, not the material instability theory, is indispensable for a description of the occurrence of necking.

A tensile test specimen keeps uniform deformation on the primary path beyond the peak point. On the other hand, necking occurs by switching to the bifurcation path on the bifurcation point immediately after the peak point [4][8][14] for the long specimen. The Hill's bifurcation criterion [9] is a mediator between the material and structural instability problems. In the Hill's criterion, the discussion of the material instability is extended to structural instability by integrating the whole volume. The Hill's bifurcation criterion is also extended to the large deformation problem [15]. In this section, equivalence between the well established Hill's bifurcation criterion for elasto-plasticity and the standard finite element bifurcation criterion is determined.

4.1 Hill's bifurcation criterion

The Hill's bifurcation criterion [9] is as follows.

$$\int_v \dot{\boldsymbol{\epsilon}}^* : \dot{\boldsymbol{\sigma}}^* dv = 0 \tag{47}$$

Where v is volume, and the right superscript $*$ indicates the difference between the bifurcation and primary solutions. In the framework of the updated Lagrangian formulation, the Hill's criterion is extended to the large deformation problem by using conjugate strain and stress rates in the previous section. The Hill's criterion can be rewritten.

$$\int_v \Big[\dot{\boldsymbol{S}}^* : \boldsymbol{D}^* + \boldsymbol{\sigma} : (\boldsymbol{L}^{*T} \cdot \boldsymbol{L}^*) \Big] dv = 0 \tag{48}$$

where the constitutive equation relating the Truesdell stress rate $\dot{\boldsymbol{S}}$ to the stretching tensor $\boldsymbol{D}$ is shown in Eq. (38). The linear comparison solid proposed by Hill [9] is introduced.

$$\dot{\boldsymbol{S}}^I = \tilde{\boldsymbol{C}}^c : \boldsymbol{D}^I \tag{49}$$

$$\dot{\boldsymbol{S}}^{II} = \tilde{\boldsymbol{C}}^c : \boldsymbol{D}^{II} \tag{50}$$

The right superscripts I and II show the primary and bifurcation solutions, respectively. $\tilde{\boldsymbol{C}}^c$ is the constitutive tensor with the linear comparison solid. The linear comparison solid is a fictional solid and assumes that yielding continues in both primary and bifurcation directions on the bifurcation point; namely, the unloading possibility is excluded. In case of an elastic state, the linear comparison solid is unnecessary and the elastic constitutive tensor is employed.

Using Eqs. (49) and (50) gives,

$$\dot{\boldsymbol{S}}^* = \tilde{\boldsymbol{C}}^c : \boldsymbol{D}^* \tag{51}$$

Substituting Eq. (51) for Eq. (48) with the standard finite element formulation gives,

$$\{\dot{U}\}^T [K^c] \{\dot{U}\} = 0 \tag{52}$$

where

$$[K^c] = [K^{mc}] + [K^g] \tag{53}$$

$$[K^{mc}] = \int_v [B^m]^T [\tilde{C}^c] [B^m] dv \tag{54}$$

$$[K^g] = \int_v [B^g]^T [\sigma] [B^g] dv \tag{55}$$

$\{\dot{U}\}$ is the nodal velocity vector. $[B^m]$ is the matrix relating the stretching $\boldsymbol{D}$ to the elemental nodal velocity $\{\dot{U}\}$, and $[B^g]$ is the matrix relating the velocity gradient $\boldsymbol{L}$ to the nodal velocity $\{\dot{U}\}$, respectively, in the finite element formulation.

Letting $[K^c]$ be the fictional tangent stiffness matrix with the linear comparison solid in Eq. (52), Hill's bifurcation criterion is written equivalently as follows.

$$\det[K^c] = 0 \tag{56}$$

4.2 Equivalency to the standard bifurcation criterion

Eq. (57) shows the rate form of the virtual work principle in the framework of the updated Lagrangian finite element formulation [16].

$$\int_v \dot{\boldsymbol{S}} : \delta \boldsymbol{D} dv + \int_v \boldsymbol{\sigma} : \frac{1}{2}(\boldsymbol{L}^T \cdot \delta \boldsymbol{L} + \delta \boldsymbol{L}^T \cdot \boldsymbol{L}) dv = \delta \dot{R} \tag{57}$$

where δ is the variation originating in the virtual work and δR is the external virtual work. Eq. (57) can be derived from the rate form of the virtual work principle for the infinitesimal deformation problem by using conjugate strain and stress rates.

The tangent stiffness matrix $[K]$ is obtained from finite element discretization of the left side in Eq. (57) with the constitutive relationship (38).

$$\text{The left side of Eq. (57)} = \{\delta \dot{U}\}^T [K] \{\dot{U}\} \tag{58}$$

where

$$[K] = [K^m] + [K^g] \tag{59}$$

$[K^g]$ in Eq. (59) is identical with Eq. (55). As for $[K^m]$, the difference from $[K^{mc}]$ in Eq.(54) is only the constitutive matrix.

$$[K^m] = \int_v [B^m]^T [\tilde{C}] [B^m] dv \tag{60}$$

In the relation, the well known standard bifurcation criterion using the complete tangent stiffness matrix $[K]$ is as follows.

$$\det[K] = 0 \tag{61}$$

In the case where unloading never occurs on the yielding points, the complete tangent stiffness matrix $[K]$ is identical to the fictional tangent stiffness matrix $[K^c]$. Therefore, the elasto-plastic bifurcation points can be evaluated conventionally only from the complete tangent stiffness excluding the unloading. There are many discussions of the elasto-plastic finite element bifurcation criterion based on Hill's theory [17][18][19][20].

I would like to emphasize that finite element analysis does not need to have a special procedure introduced to evaluate the elasto-plastic bifurcation points. The reason is as follows. On each convergent equilibrium point, the complete

tangent stiffness matrix is assembled supposing that yielding continues on plastic integration points. By checking the singularity of this complete tangent stiffness, the passage of the elasto-plastic bifurcation points can be monitored. It should be kept in mind that the above procedure implicitly includes Hill's criterion [9]. The lack of a need for the Hill's criterion for the elasto-plastic bifurcation has been discussed in other contexts [21].

5 Computational analyses

As previously mentioned, the peak point even with the hardening true stress-strain relationship with a uniformly deformed state and necking immediately after the peak point, can be simulated by the structural bifurcation analysis. The conventional arc-length control [22] can climb over the peak point. However, switching to the bifurcation path is necessary for post-necking analysis after detecting the bifurcation points. This section is devoted to describing a sophisticated computational strategy for necking localization.

5.1 Computational strategy for branch-switching

On the bifurcation point, the bifurcation incremental displacement vector $\{\Delta U^{II}\}$ is as follows with the primary incremental displacement vector $\{\Delta U^{I}\}$ and the critical eigenvector of the tangent stiffness matrix $\{\theta\}$ [23].

$$\{\Delta U^{II}\} = \{\Delta U^{I}\} + \alpha\{\theta\} \tag{62}$$

Where α is a scaling factor of the critical eigenvector $\{\theta\}$. The scaling factor α of the critical eigenvector $\{\theta\}$ in Eq. (62) is essential and must be chosen carefully for the finite element bifurcation analysis. A trial-and-error approach to determine the magnitude of the scaling factor is necessary for elastic branch-switching in general. Contrarily, the scaling factor α can be determined effectively in elasto-plasticity. Because the unloading possibility is excluded for the evaluated bifurcation point in the present bifurcation criterion, unloading must not occur at the moment of branching. Hence, the scaling factor α may be determined so that it brings no unloading. Furthermore, the obtained equilibrium points may return again to the primary path in the case of a too small scaling factor α. Unloading occurs during tracing of the bifurcation path where the direction of deformation suddenly changes, even if unloading does not occur at the moment of branching. In the numerical procedure, as the largest or the most appropriate scaling factor α can be determine so that the first unloading point remains neutral [24].

An in-house finite element code is implemented for the necking bifurcation

analysis. This is because commercial finite element codes cannot treat bifurcation problems without imperfection. The J_2 flow theory is adopted for the elasto-plastic constitutive equation. The following uniaxial relationship between the equivalent true stress $\bar{\sigma}$ and the equivalent plastic strain $\bar{\varepsilon}^p$ is assumed in the plastic range.

$$\bar{\sigma} = \sigma_y \left(1 + \frac{\bar{\varepsilon}^p}{\varepsilon_y}\right)^n \tag{63}$$

$$e_y = \frac{\sigma_y}{E} = \frac{1}{500} \tag{64}$$

where σ_y is the yield stress and ε_y is the yield strain. The calculations set the elastic modulus as $E = 200$ (GPa) and the Poisson's ratio as $\nu = 0.333$. The hardening true stress-strain relationship is assumed by using $n = 0.0625$ in Eq. (63), and the material softening effect is completely excluded.

5.2 Two-dimensional necking localization analyses

Fig.3 shows a two-dimensional analysis model. Only one quarter is analyzed because of the symmetric shape and deformation. A 4-node bi-linear isoparametric element is used for the finite element. A tension force is applied to the non-frictional edge of the solid so that constant displacement along the edge is achieved. The plane strain and plane stress models are computed.

For the numerical integration of the isoparametric element in the plane strain state, the selective reduced integration method is used to avoid volumetric locking [25]. Fig.4 depicts the calculated equilibrium path in the plane strain state. Although deformation is uniform in the whole solid, the peak point • exists even with the hardening true stress-strain relationship. This is because a decrease in the cross-sectional area reduces the axial internal force [12]. Beyond the peak point, the bifurcation point ∘ is detected and the equilibrium path branches. Uniform deformation continues and the whole solid yields even beyond the bifurcation point on the primary path. Branch-switching is initiated using the critical eigenvector; a dotted line in Fig.4 shows the switched bifurcation path. Fig.5 shows a deformed configuration on the bifurcation path. The necking bifurcation causes unloading from the edge and the unloading zone extends to the center of the solid. Therefore, the unloading (elastic) zone is hardly deformed and the plastic strain is localized into the central plastic zone. This naturally implies that diffuse necking can be simulated.

However, for a plane stress state, a completely full numerically integrated isoparametric element is utilized. One reason for this is that the plane stress state is free from the volumetric locking due to the zero stress state in the direction of the thickness. Fig. 6 depicts the equilibrium paths in the plane

stress state. Similar to the plane strain state in Fig.4, the bifurcation point is detected immediately beyond the peak point. Fig.7 shows the deformation on the switched bifurcation path, and cross-diagonal localized necking is observed. The progress of the unloading has much influence on the occurrence of cross-diagonal localized necking. In the plane stress state, the unloading again starts from the center after occurring at the edge of the solid. From this, it follows that a narrow plastic zone between the unloading zones is left and deformation is localized into the cross-diagonal plastic zone. Although cross-diagonal localized necking is observed in the plane stress state, the calculated critical eigenvector indicates the diffuse mode.

5.3 Three-dimensional necking localization analyses

Although three-dimensional necking mode has been discussed previously [26], the present computational strategy is applied to the thin and thick three-dimensional solids. Fig.8 shows a three-dimensional analysis model. Due to the symmetric shape and deformation, only one-eighth is analyzed. In three-dimensional analyses, thin and thick solids are computed. The rectangular cross-sectional width-thickness ratios (w/t in Fig.8) of thin and thick solids are 20 and 4, respectively. The three-dimensional 8-node tri-linear isoparametric element with the selective reduced integration is adopted to avoid volumetric locking [25]. A tension force with a boundary condition for the uniform deformation is applied [27].

Similarly to the previous two-dimensional analyses, bifurcation occurs immediately subsequent to the peak point. The ultimate localized modes depend on the width-thickness ratio of the solids. Fig.9 illustrates the ultimate deformed configuration of thin solid on the switched bifurcation path. In a three-dimensional thin solid, the stress state is similar to the two-dimensional plane stress state. Therefore, the cross-diagonal localized necking is simulated like Fig.7. By contrast, in the thick solid, the necking in the direction of the thickness occurs vertically in a narrow area as shown in Fig.10. This can be restated as in thick solid, dimple localized necking is simulated instead of diagonal localized necking.

Let us recall that cross-diagonal localized necking for the thin solid or dimple localized necking for the thick solid occurs. In particular, two-dimensional analysis cannot simulate dimple localized necking of the thick solid. This result of this is that three-dimensional analysis is indispensable to explain the phenomenon of necking localization.

6 Conclusions

The necking localization mechanism by structural bifurcation approach has been investigated. I explain the occurrence of the peak point in a ductile solid by treating from a one-dimensional state to a general state. By introducing full geometrical nonlinearity, the peak point can be simulated with a uniformly deformed state even with the hardening true stress-strain relationship. However, the standard full nonlinear finite element code cannot attain the occurrence of necking because necking behavior is a structural bifurcation instability problem instead of material instability. By switching to the bifurcation path, necking, in particular localized necking for the three-dimensional analysis, without imperfection can be simulated.

References

[1] J. Christoffersen and J.W. Hutchinson, A class of phenomenological corner theories of plasticity. *J. Mech. Phys. Solids.* 25, 465-487 (1979).

[2] A.L. Gurson, Continuum theory of ductile rupture by void nucleation and growth: Part I - Yield criteria and flow rules for porous ductile media. *J. Engrg. Mate. Technology.*, ASME. 99, 2-15 (1977).

[3] A. Needleman, Dynamic shear band development in plane strain. *J. Appl. Mech.*, ASME. 56, 1-9 (1989).

[4] V. Tvergaard, A. Needleman and K.K. Lo, Flow localization in the plane strain tensile test. *J. Mech. Phys. Solids.*, 29, 115-142 (1981).

[5] V. Tvergaard and A. Needleman, Analysis of the cup-cone fracture in a round tensile bar. *Acta Metallurgica*, 32, 157-169 (1984).

[6] S. Nemat-Nasser, Phenomenological theories of elastoplasticity and strain localization at high strain rates. *Appl. Mech. Reviews*, 45, S19-S45 (1992).

[7] H. Petryk and K. Thermann, On discretized plasticity problem with bifurcation. *Int. J. Solids Struct.*, 29, 745-765 (1992).

[8] R. Hill and J.W. Hutchinson, Bifurcation phenomena in the plane tension test. *J. Mech. Phys. Solids*, 23, 239-264 (1975).

[9] R. Hill, A general theory of uniqueness and stability in elastic-plastic solids, *J. Mech. Phys. Solids*, 6, 236-249 (1958).

[10] D.M. Norris, B. Moran Jr., J.K. Scudder and D.F. Quinones, A computer simulation of the tension test, *J. Mech. Phys. Solids*, 26, 1-19 (1978).

[11] M.A. Burke and W.D. Nix, A numerical study of necking in the plane tension test, *Int. J. Solids Struct.*, 15, 379-393 (1979).

[12] H.W. Swift, Plastic instability under plane stress, *J. Mech. Phys. Solids*, 1, 1-18 (1952).

[13] E. Giessen and R. Borst, Introduction to material instabilities in solids, in *Material Instabilities in Solids*, John Wiley & Sons (1998).

[14] A. Considère, 1885 A.G. Considère, Memoire sur l 'Emploi du Fer et de l 'Acier dans les Constructions, Annales des Ponts et Chausses, 9, 574-775 (1885).

[15] J. Rice, The localization of plastic deformation, in *Theoretical, Applied Mechanics*, North-Holland, 207-220 (1977).

[16] K.J. Bathe, *Finite Element Procedures*, Prentice Hall (1996).

[17] J.P. Bardet, Finite element analysis of plane strain bifurcation within compressible solids, *Comp. Struct.*, 36, 993-1007 (1990).

[18] Y. Goto, S. Suzuki and W.F. Chen, Analysis of critical behavior of semi-rigid frames with or without load history in connections, *Int. J. Solids Struct.*, 27, 467-483 (1991).

[19] Y.M. Leroy and O. Chapuis, Localization in strain-rate-dependent solids, *Comp. Methods in Appl. Mech., Engrg.*, 90, 969-986 (1991).

[20] S.Q. Nguyen and N. Triantafyllidis, Plastic bifurcation, postbifurcation analysis for generalized standard continua, *J. Mech. Phys. Solids*, 37, 545-566 (1989).

[21] P. Wriggers and J.C. Simo, General procedure for the direct computation of turning, bifurcation points, *Int. J. Numer. Methods in Engrg.*, 30, 155-176 (1990).

[22] Crisfield M.A. *Non-linear Finite Element Analysis of Solids, Structures*, Volume 1 Essentials, John Wiley & Sons (1991).

[23] F. Fujii F. and S. Okazawa, Pinpointing bifurcation points and branch-switching, *J. Engrg. Mech.*, ASCE, 123, 179-189 (1997).

[24] J.W. Hutchinson, Post-bifurcation behavior in the plastic range, *J. Mech. Phys. Solids*, 21, 163-190 (1973).

[25] T.J.R. Hughes, Generalization of selective integration procedures to anisotropic and nonlinear media, *Int. J. Numer. Methods in Engrg.*, 15, 1413-1418 (1980).

[26] V. Tvergaard, Necking in tensile bars with rectangular cross-section, *Comp. Methods in Appl. Mech., Engrg.*, 103, 273-290 (1993).

[27] M. Zbib and J.S. Jubran, Dynamic shear banding: a three-dimensional analysis, *Int. J. Plasticity*, 8, 619-641 (1992).

List of Figures and Tables

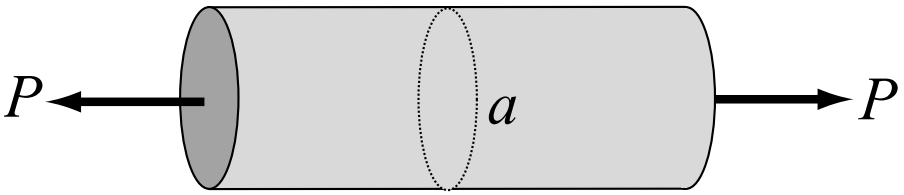

Fig. 1. One-dimensional ductile member

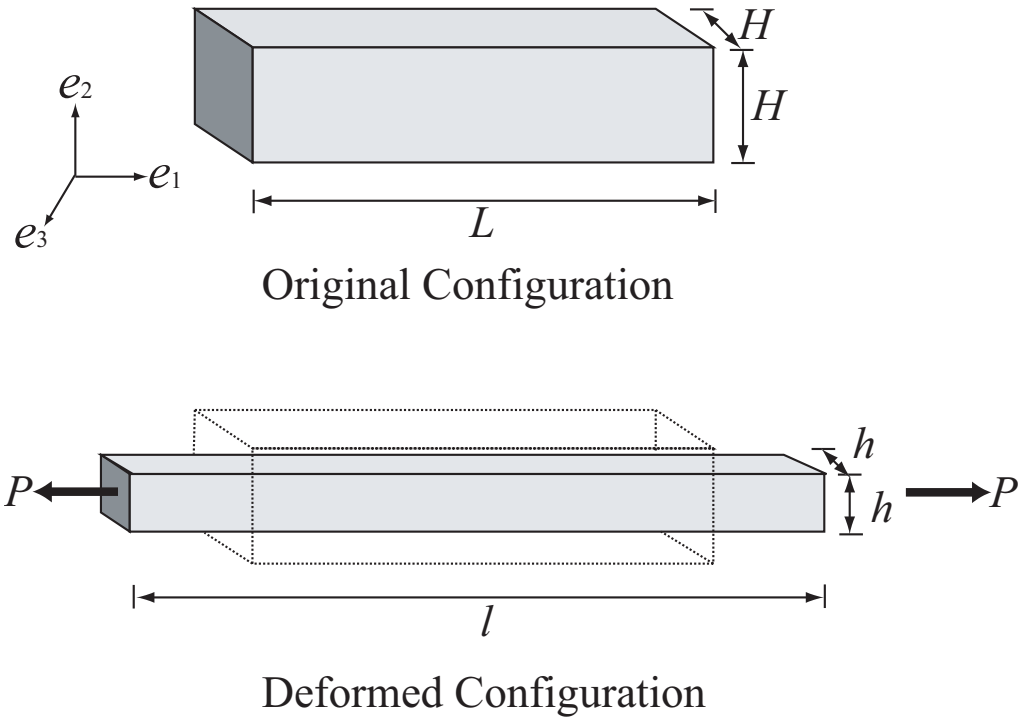

Fig. 2. Deformation of ductile member with a square cross-section

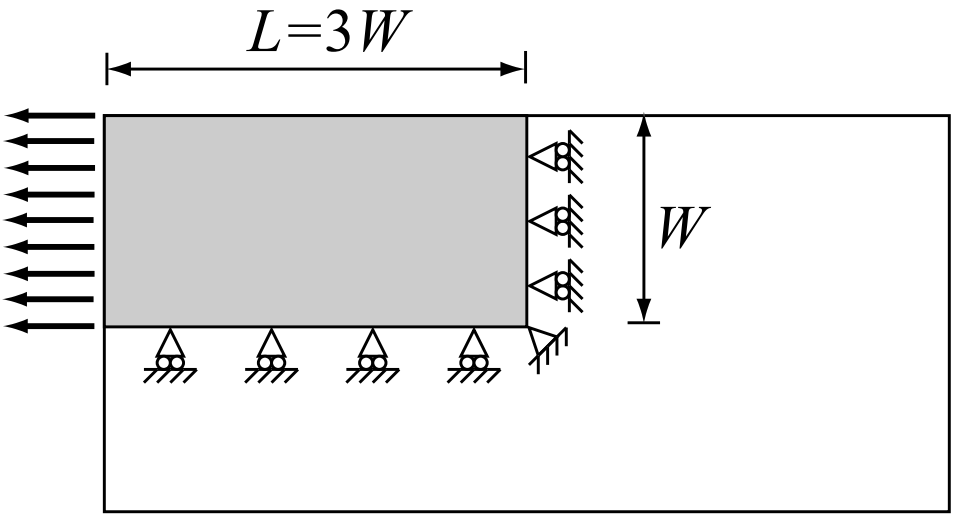

Fig. 3. Two-dimensional analysis model

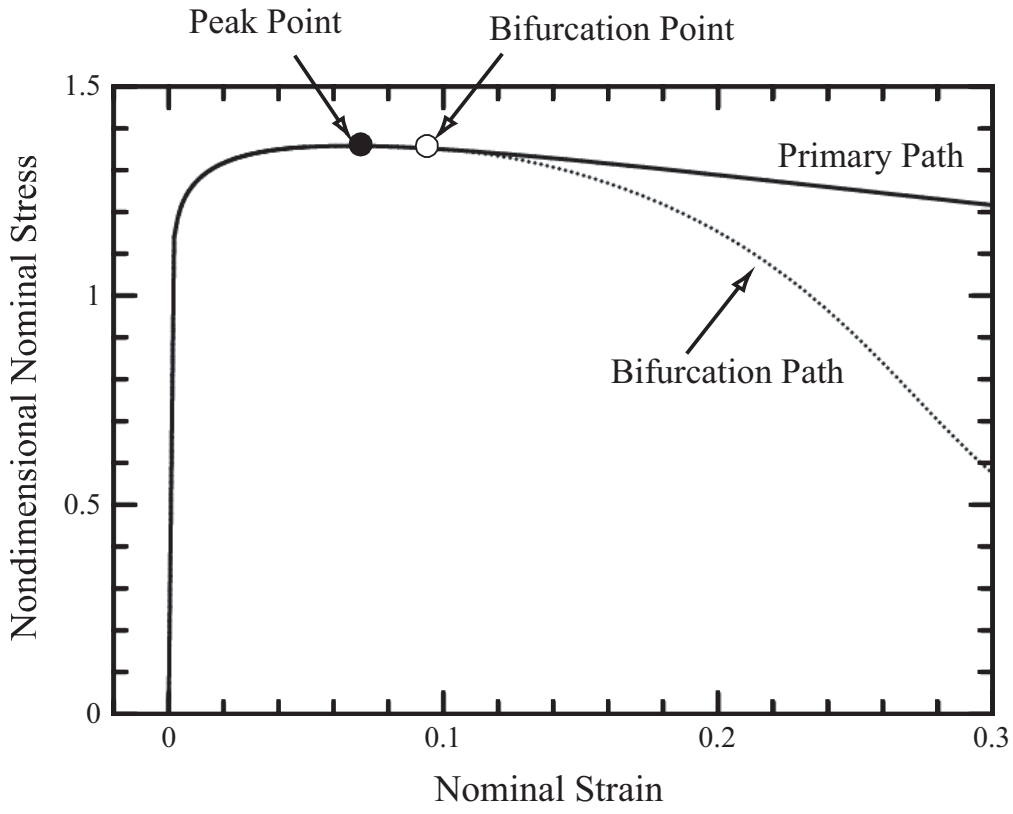

Fig. 4. Equilibrium path in the plane strain state

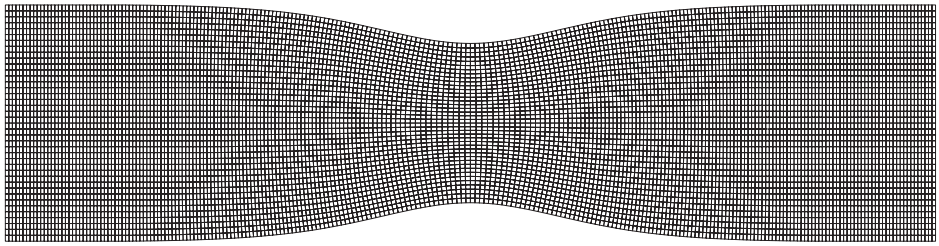

Fig. 5. Diffuse necking on the bifurcation path in the plane strain state

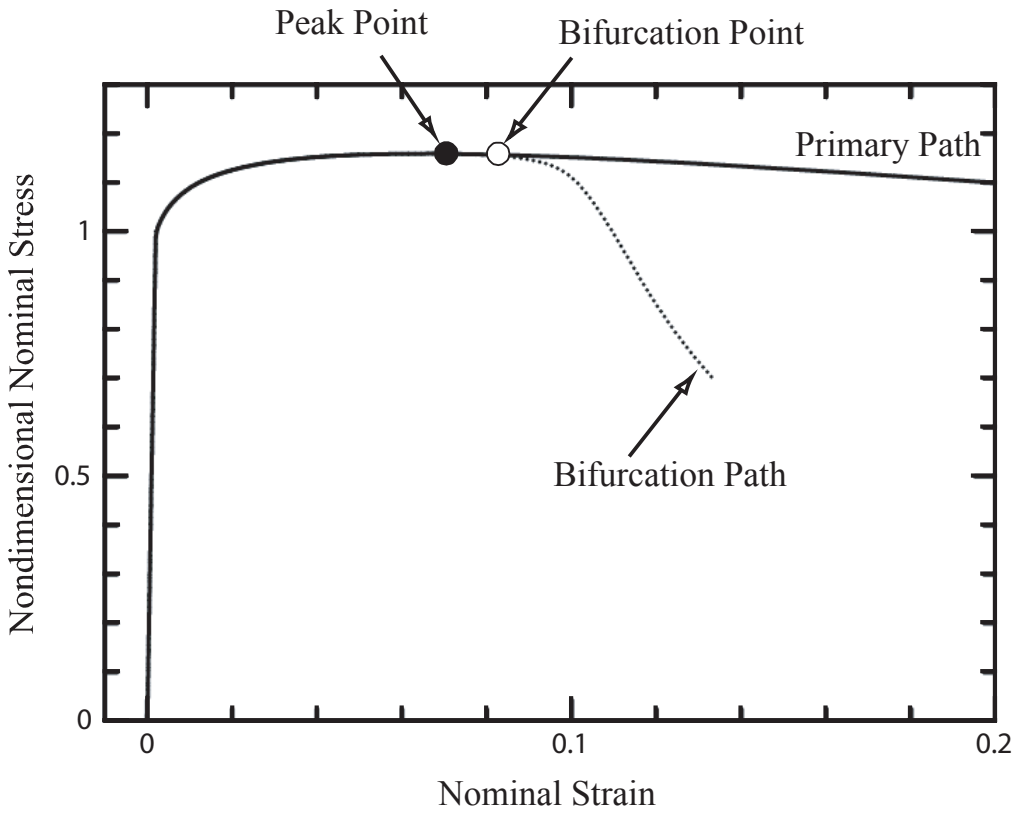

Fig. 6. Equilibrium path in the plane stress state

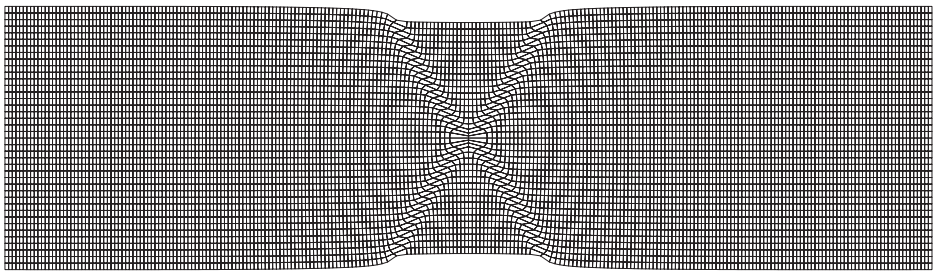

Fig. 7. Cross-diagonal localized necking on the bifurcation path in the plane stress state

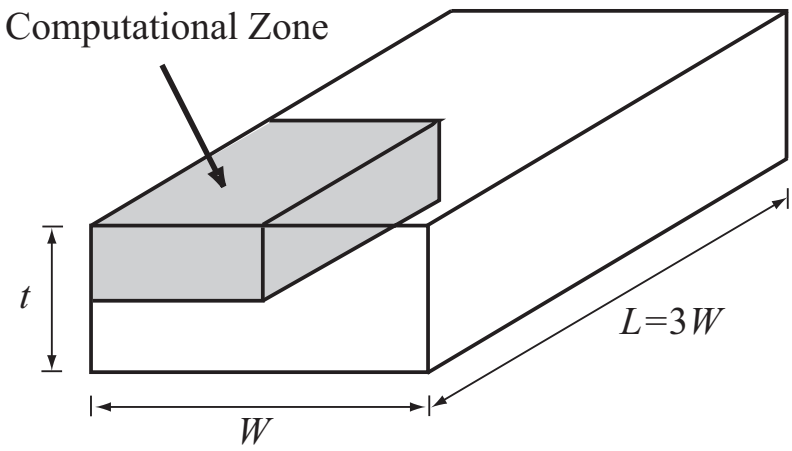

Fig. 8. Three-dimensional analysis model

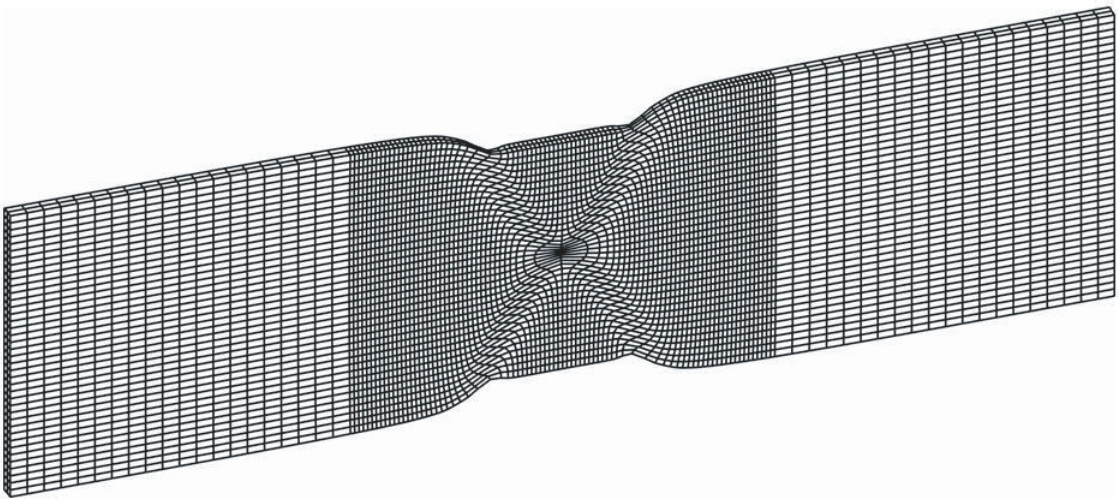

Fig. 9. Cross-diagonal localized necking of thin solid

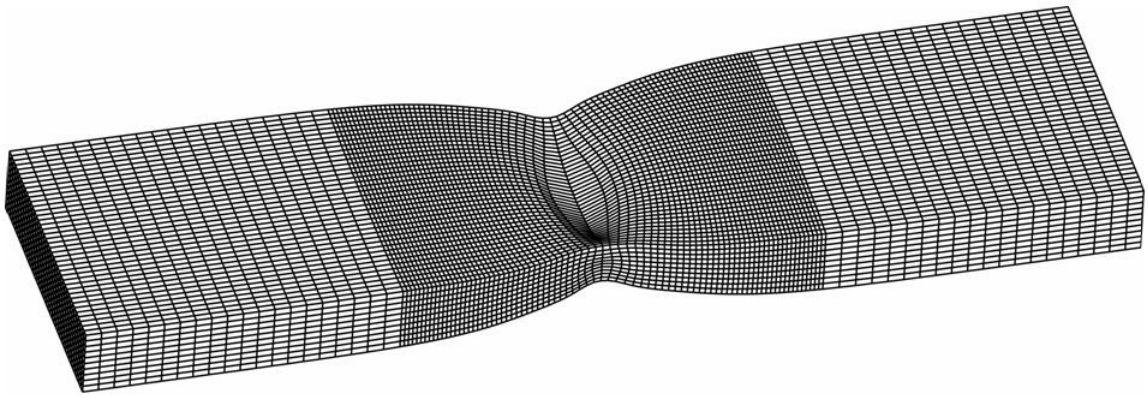

Fig. 10. Dimple localized necking of thick solid